Available online at www.sciencedirect.com
SCIENCE DIRECT®
Journal of Magnetic Resonance 170 (2004) 228–235
JMR Journal of Magnetic Resonance
www.elsevier.com/locate/jmr

Effect of magnetic field gradients induced by microvasculature on NMR measurements of molecular self-diffusion in biological tissues

V.G. Kiselev*

Medical Physics, Department of Diagnostic Radiology, University Hospital Freiburg, Hugstetterstr. 55, D-79106, Freiburg, Germany

Received 2 March 2004; revised 1 July 2004
Available online 29 July 2004

Abstract

Presence of induced mesoscopic gradients of magnetic field in magnetically heterogeneous samples affects the measured value of apparent diffusion coefficient. This effect is investigated theoretically in the context of diffusion measurements in perfused biological tissues with blood as the paramagnetic compartment. It is shown that the apparent diffusion coefficient is sensitive to mutual correlations in vessel positions. Neglect of these correlations results in a failure of the commonly used model of microvasculature in which vessels are described as independently placed cylinders. The model is modified to account for intervessel correlations. The results indicate an underestimation of apparent diffusion coefficient in proportion to the magnetic susceptibility of intravascular compartment in agreement with published experimental data. The proportionality coefficient depends on the microvascular architecture. Comparison with experimental data yields a numerical value for a new model parameter that characterises the correlation in mutual positions of blood vessels.

Keywords: Diffusion; Apparent diffusion coefficient; Vascular network; Contrast agent; Heterogeneous media

1. Introduction

Determination of diffusion coefficient by NMR is accomplished by comparison of a measured signal response to applied gradient of magnetic field with a theoretical prediction obtained for homogeneous medium. This method faces a problem when applied to magnetically heterogeneous media such as biological tissues in which the actually present gradients can hardly be monitored. The intrinsic magnetic inhomogeneity of living tissues arises from blood which is paramagnetic in its deoxygenated state. When exposed to the strong magnetic field, the blood vessels induce mesoscopic fields thus changing the local value of the applied gradient. Hereafter, the mesoscopic scale implies the lengths of the order of the size of cells and small vessels (several micrometer and above) in contrast to the microscopic scale of molecular processes and to the macroscopic dimensions of imaging (of the order of millimeter and above). For example, a capillary of radius 3.5 μm in the field 1.5 T creates the local gradient up to 200 mT/m, which is stronger than the typically used diffusion weighting gradients in human studies. A consistent theory for interpretation of diffusion measurement in magnetically heterogeneous media is currently not available.

Zhong, Kennan, and Gore [1] demonstrated an appreciable effect of mesoscopic gradients. They found that doping bulk blood with an extracellular contrast agent increases the echo magnitude in presence of diffusion weighting. This counterintuitive result was explained by the effect of regions in which the applied gradient was compensated by the susceptibility induced ones. Assumption of Gaussian distribution of mesoscopic gradients helped to understand the effect in

* Fax: +49-761-2703831.
E-mail address: kiselev@ukl.uni-freiburg.de.

1090-7807/$ - see front matter © 2004 Elsevier Inc. All rights reserved.
doi:10.1016/j.jmr.2004.07.004

frames of a theoretical model, although this model, being unrealistic, could not provide a satisfactory quantitative description. Neither it had a prediction capability because of the necessary adjustment of internal parameters to experimental data.

Similar effect was discovered by the same group in animal experiments [2]. It was found that there was a linear dependence between the relative increase in the apparent diffusion coefficient in the rat brain and the intravascular magnetic susceptibility with a coefficient 33%/ppm. A quantitative theory of this effect is currently lacking.

The effect of background gradients can be reduced by replacing the constant segments of the applied gradient with a train of alternated gradient pulses interleaved with refocusing pulses [3]. This increases significantly the quality of diffusion-weighted imaging at the cost of reduced weighting [4].

The idea motivating this study is inferring information about the morphological properties of microvessels from the measured effect of the background gradients. This is only possible with a quantitative theory at hand. To build such a theory is the aim of the present study.

This paper is structured as follows. The problem is first analysed within the available theory of transverse relaxation in the microvascular network [5–7]. Although successful in the absence of diffusion weighting, the involved tissue model fails to yield reasonable results for a sufficiently strong diffusion weighting. Analysis show that this happens due to the neglect of correlations in the mutual positions of vessels. A new modified model is proposed. It results in a reasonable agreement with the available experimental data and predicts a dependence of signal attenuation on details of microvascular architecture.

2. Tissue model

Investigated tissue is treated as a macroscopically homogeneous and isotropic medium. Mesoscopic inhomogeneities arise from the microvasculature which is modeled with a large number N of randomly positioned and oriented straight infinite cylinders [5–7]. The cylinder positions are statistically independent in the original model [5–7], which is hereafter referred to as the model of independent cylinders. The cylinders, which are characterized by their magnetic susceptibility χ and radius ρ, occupy a fraction ζ of the total volume. The diffusion in the parenchyma is assumed to be free with an effective constant D. Throughout this study the intravascular signal is neglected, due to the small blood volume fraction, the suppression of signal from moving blood at large b-factors and the presence of an intravascular contrast agent discussed below.

The following default values are used in performed numerical calculations. $D = 0.8\,\mu m^2/ms$, which is close to the observed apparent diffusion coefficient in the human brain [8], $\chi = 0.43 \times 10^{-7}$ in the SGC units for blood deoxygenated by 40% [9]. The blood volume fraction in the arterial, capillary, and venous pools is assumed to be 0.5, 2, and 1%, respectively. The apparent smallness of these values is specific for NMR imaging as discussed in [10]. The variation of magnetic susceptibility in capillaries between their arterial and venous ends is roughly simulated by accounting only for a half of capillaries. This gives an effective volume fraction of paramagnetic blood $\zeta = 2\%$. The effective radius of monosized cylinders is calculated by averaging $\rho^{-2/3}$ as discussed in [10]. This results in $\rho = 8.5\,\mu m$. All three blood pools are taken into account in simulating the effect of paramagnetic blood pool contrast agent. This gives $\zeta = 3.5\%$ and $\rho = 7.2\,\mu m$. The blood magnetic susceptibility in this case is assumed to be 10-fold increased and equal in all pools: $\chi = 4.3 \times 10^{-7}$.

3. Signal attenuation in magnetically inhomogeneous tissues

Interpretation of diffusion measurements is based on a linear exponential dependence of the NMR signal, s, on the diffusion coefficient D

$$s = s_0 e^{-b_0 D}. \tag{1}$$

Here s_0 is the signal in the absence of diffusion weighting, the quantity b_0, which is called the b-factor, depends on the applied gradient and the involved pulse sequence. In the present paper, the Stejskal–Tanner pulse sequence [11] is considered for which

$$b_0 = G_0^2 \delta^2 \cdot \left(\Delta - \frac{\delta}{3} \right) \tag{2}$$

in homogeneous media. Here G_0 is the magnitude of the applied gradient $\mathbf{G}_0$ of the local cyclic Larmor frequency. It is measured, for example, in s^{-1}/m. Throughout this paper, the bold and the corresponding cursive letters denote vectors and their magnitudes, respectively. The present analysis is restricted to the gradient applied in the direction of the main magnetic field, $\mathbf{B}_0$. The timing parameters δ and Δ define the duration of the gradient pulse and the diffusion time (Fig. 1A). The following values are used as the default parameters for numerical calculations simulating the diffusion measurements at $B_0 = 1.5\,T$ with a strong diffusion weighting: $G_0 = 40\,mT/m$, $\delta = 40\,ms$, $\Delta = 45\,ms$, and $T_E = 100\,ms$.

Magnetic field gradient experienced by spins in the inhomogeneous media differ from $\mathbf{G}_0$ by the locally induced gradient, $\mathbf{G}_1$. The diffusion weighting reduces the magnetization of individual spin packets by e^{-bD} with a position-dependent b-factor, b. The total signal is found by the averaging over all positions and orientation of paramagnetic vessels:

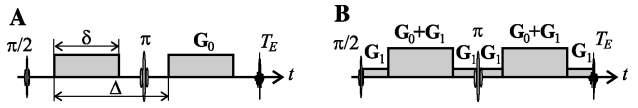

Fig. 1. Symbolic representation of the Stejskal–Tanner pulse sequence. Transverse signal is excited by the $\pi/2$ pulse, refocused by the π pulse and recorded at the echo time, T_E. (A) Shows the applied pulse sequence. Gradient $\mathbf{G}_0$ is acting during time δ, the diffusion time is Δ. The b-factor for homogeneous media is given by Eq. (2). (B) Illustrates the gradient experienced by spins in the magnetically inhomogeneous media. For the same timing, the diffusion weighting is provided by the sum of applied gradient $\mathbf{G}_0$ and a constant component $\mathbf{G}_1$ which is induced by the heterogeneous magnetic susceptibility. The b-factor is given by Eq. (4).

$$s = s_0\langle \mathrm{e}^{-bD}\rangle. \tag{3}$$

The present analysis is applied to the case of static dephasing in which $\mathbf{G}_1$ changes over distances, which are longer than the diffusion length of the spin bearing molecules. This allows for treating $\mathbf{G}_1$ as a constant for each individual spin (Fig. 1B). A straightforward calculation for the pulse sequence shown in Fig. 1B results in

$$b = b_0 + \mathbf{G}_0\mathbf{G}_1\delta\cdot\left(\Delta - \frac{\delta}{3}\right)\left(T_\mathrm{E} - \frac{\Delta-\delta}{2}\right) + \frac{\mathbf{G}_1^2 T_\mathrm{E}^3}{12}, \tag{4}$$

where b_0 is given by Eq. (2).

The mesoscopic gradient $\mathbf{G}_1$ is a sum of gradients induced by individual vessels

$$\mathbf{G}_1 = \sum_n \mathbf{g}_n, \tag{5}$$

where $n = 1,\ldots,N$ counts all vessels, which are described as infinite straight cylinders (Section 2). Each cylinder contributes the following value to the local Larmor frequency

$$\omega_n = \delta\omega\frac{\rho_n^2}{r_n^2}\cos 2\phi_n \sin^2\theta_n. \tag{6}$$

Here $\delta\omega = 2\pi\chi\gamma B_0$ is the maximal deviation from the Larmor frequency on the cylinder surface, with γ denoting the gyromagnetic ratio. Other notations are explained in Fig. 2. Finally, $\mathbf{g}_n = \nabla\omega_n$ provides an explicit expression to be used in Eq. (4).

The averaging of Eq. (4) over the vessel positions is hindered by the presence of terms with $m \neq n$ in the sum

$$\mathbf{G}_1^2 = \sum_{m,n}\mathbf{g}_m\mathbf{g}_n. \tag{7}$$

This sum can be approximated by its diagonal part with $n = m$ provided the volume fraction of blood, ζ, is low, which is a good assumption for the majority of organs, in which ζ is a few per cent. In such tissues, the vessels are separated by distances, which are typically larger than their diameters. The cross-terms with $m \neq n$ in the double sum in Eq. (7) are then everywhere small, since they are products of two factors that peak near different vessels. The smallness of these terms

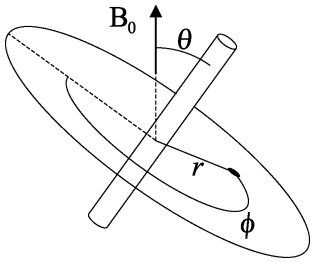

Fig. 2. Geometric parameters associated with individual cylinders. The cylinder of radius ρ forms the angle θ with $\mathbf{B}_0$. The polar coordinates in the plane, which is normal to the cylinder, are specified by the distance r and the angle ϕ. The latter is measured from the projection of the main field. All parameters acquire subscript n in Eq. (6).

alone is not sufficient to neglect them, since their number is proportional to N^2, which is much larger than N, the number of diagonal terms. Omitting the cross-terms is made possible by an observation that the sum over the vicinity of a given vessel converges: $\mathbf{g}_n\sum_m \mathbf{g}_m < \infty$. Thus, the actual contribution of these terms is proportional to N rather than N^2. The convergence follows from the fact that the gradient induced by a single vessel is inversely proportional to the third power of separation r from the vessel, Eq. (6). The independence of the cross-terms on the applied gradient suggests that their contribution in the signal attenuation should be relatively small for large $\mathbf{G}_0$. However, this is only true provided the configurations with closely situated vessels give a small contribution to the signal proportionally to their low statistical weight. This condition can be violated as discussed below in Section 5.

Neglecting the intervessel cross-terms gives the following approximate form to $\mathbf{G}_1^2$

$$\mathbf{G}_1^2 \approx \sum_n \mathbf{g}_n^2. \tag{8}$$

Substitution of this expression in Eq. (4) results in the following decomposition of e^{-bD} in factors contributed by individual vessels:

$$\mathrm{e}^{-bD} \approx \mathrm{e}^{-b_0 D}\prod_n \psi_n. \tag{9}$$

Here b_0 is deterministic, not subjected to averaging. It would be the experimental b-factor in the magnetically homogeneous sample. The quantity ψ_n arising from the nth vessel takes the form

$$\begin{aligned}\ln\psi_n &= -(b-b_0)D \\ &= -D\mathbf{G}_0\mathbf{g}_n\delta\cdot\left(\Delta-\frac{\delta}{3}\right)\left(T_\mathrm{E}-\frac{\Delta-\delta}{2}\right) - \frac{D\mathbf{g}_n^2 T_\mathrm{E}^3}{12}\end{aligned} \tag{10}$$

according to Eq. (4). This expression is the subject to the statistical averaging as discussed below.

4. Averaging over independent vessel positions

Statistical independence of cylinders assumed in model [5–7] simplifies the averaging over their positions. The mean value of product in Eq. (9) is the product of the mean values:

$$s = s_0 \mathrm{e}^{-b_0 D} \prod_n \langle \psi_n \rangle. \tag{11}$$

Each factor $\langle \psi_n \rangle$ is the averaged effect of a single vessel on the spin packet magnetization. It takes the following form [5–7]

$$\begin{aligned} \langle \psi \rangle &= \int \frac{\mathrm{d}o}{4\pi} \int \frac{\mathrm{d}^2\mathbf{x}}{A} \psi \\ &= 1 - \frac{\pi\rho^2}{A} \int \frac{\mathrm{d}o}{4\pi} \int \frac{\mathrm{d}^2 x}{\pi\rho^2} (1 - \psi). \end{aligned} \tag{12}$$

Here, the integration $\int \mathrm{d}o/4\pi$ performs the averaging over the vessel orientations. It can incorporate if necessary the averaging over its radius and other parameters such as, e.g., its magnetic susceptibility. The inner integral fulfills the averaging over the vessel position in the plane, which is orthogonal to the vessel (Fig. 2). This plane crosses the entire sample over a macroscopic area A. The transition between the two integral forms in Eq. (12) occurs by the substitution $\psi = 1 - (1 - \psi)$. The subscript n in ψ_n is omitted for simplicity.

The ratio $\pi\rho^2/A$ in Eq. (12) is the fraction of volume occupied by the single vessel. As this value is very small, one can convert the last expression in Eq. (12) into an exponential function, substitute it in Eq. (11) and calculate the product [5]. This results in the following form of the signal

$$\ln \frac{s}{s_0} = -b_0 D - \zeta \int \frac{\mathrm{d}o}{4\pi} \int \frac{\mathrm{d}^2\mathbf{x}}{\pi\rho^2} (1 - \psi), \tag{13}$$

where $\zeta = \pi\rho^2 N/A$ is the volume fraction occupied by all vessels. This is the basic formula of the previously developed theory [5–7]. Its application to the considered problem is achieved by accounting for the applied gradient in attenuation factor ψ according to Eq. (10).

5. Results for model of independent cylinders

Numerical evaluation of integral in Eq. (13) yields the signal, which can be considered as a function of b-factor Eq. (2). This function shows a rapid exponential increase in the signal for large b-factors such that $b_0 D \geqslant 1$ (Fig. 3). An estimate gives in the limit $b_0 D \gg 1$

$$\ln s \approx 0.657 \zeta \frac{\delta\omega T_\mathrm{E}}{(\delta\omega t_D)^{1/3}} \frac{\mathrm{e}^u}{u}, \tag{14}$$

where

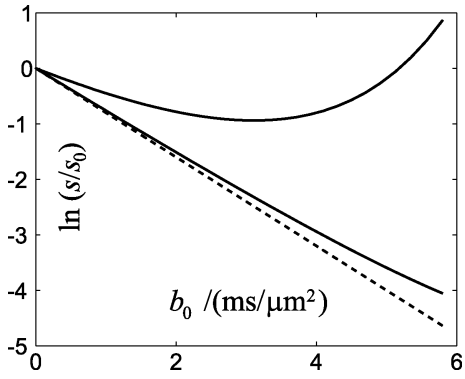

Fig. 3. Logarithm of signal attenuation as a function of b-factor Eq. (2) as predicted by the model of independent cylinders. The dashed line shows the function $-b_0 D$ which is expected in homogeneous samples. The nearly straight solid line is the model prediction for the default parameters defined in Section 2 and after Eq. (2). The upper line represents the calculated signal in the presence of the blood pool contrast agent as described in Section 2. The unrealistic increase in the signal for large b_0 is due to overlapping vessels as discussed in the text.

$$u = 4 b_0 D \cdot \left(\frac{\Delta}{T_\mathrm{E}} - \frac{\delta}{3T_\mathrm{E}} \right) \left(1 - \frac{\Delta - \delta}{2T_\mathrm{E}} \right)^2. \tag{15}$$

This indicates that the model of independent cylinders faces a serious problem which is discussed in the rest of this section.

The failure to give reasonable results is related to configurations with overlapping cylinders. Such configurations are not present in the real vascular network, but they are allowed in the model. According to the model, two completely overlapping cylinders create a twofold stronger magnetic field, which is unrealistic. This drawback does not cause any problem for modeling the signal relaxation in the absence of the diffusion weighting [5–7], since such configurations contribute proportionally to their low statistical weight. This proportionality is insured by the restricted contribution of individual vessels: $\psi < 1$ according to Eq. (10) for $G_0 = 0$. The weight is proportional to the factor ζ^2. For the typical MR imaging and tissues with $\zeta < 0.1$, this value is negligible, since it is below the noise level.

In the presence of strong diffusion weighting, contributions ψ_n of individual vessels in Eq. (9) can become exponentially large limited to $\psi_n < \mathrm{e}^{+b_0 D}$. This happens for spin packets located in the regions in which a partial compensation occurs between the applied and the induced gradients ($\mathbf{G}_0\mathbf{g}_n < 0$ in Eq. (10)). The exponential increase in their contribution to the signal overrides the small statistical weight of the favorable configurations of vessels. The extent of the gradient compensation in the field of a single vessel is limited by the restricted value of the induced gradient whose maximum is $2\delta\omega/\rho$. This limit is pushed aside by overlapping cylinders. A sufficiently large number of coinciding cylinders can compensate for any given external gradient. The results in the unrealistic signal increase.

This increase seen in Fig. 3 is too unrealistic, since the signal hitts the obvious limit $s < s_0$. This limit would be preserved in the full theory, in which the cross-terms with $m \neq n$ in Eq. (7) would balance against the large positive contributions. In the present model these terms have been omitted in the transition from Eq. (7) to Eq. (8) for the sake of independent averaging over cylinder positions Eq. (11). Note that the account for the cross-terms would not change qualitatively the significant increase in the signal at large b, since this effect follows from the statistical properties of the model.

6. Model of mutually avoiding cylinders

Let us construct a model of microvasculature in which the advantage of independent averaging over vessels is preserved, but the probability of cylinder overlapping is reduced. It will be referred to as the model of mutually avoiding cylinders. Consider first the parallel cylinders the positions of which are defined by their cross-sections with the orthogonal plane (Fig. 4A). Let us divide this two-dimensional space in cells (Fig. 4B). Each cell may be either vacant or occupied by a single vessel. Let the occupation probability be p and the cell area be σ. The appearance of the stochastic vessel distribution is now achieved by random independent occupation of the predetermined cells.

As above, the measured signal is proportional to the average factor $\langle e^{-bD}\rangle$ in the magnetization of spin packet located at the origin (Fig. 4). The factorization of this quantity expressed by Eq. (9) holds. It is convenient to extend the product in Eq. (9) to the whole lattice assuming that each empty cell contributes a factor of unity. Then the averaging in $\langle e^{-bD}\rangle$ can be performed independently for each cell with the result

$$s = s_0 e^{-b_0 D} \prod_{\alpha} [(1-p) + p\psi_\alpha]. \tag{16}$$

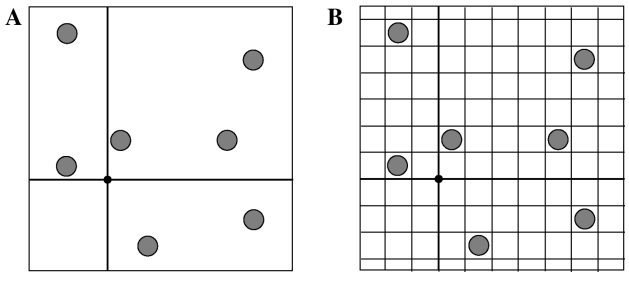

Fig. 4. Model of mutually avoiding cylinders for the simplified case of their parallel alinement. The reference frame is shown with the thick line crossing. The spin packet, the magnetization of which is studied, is shown with a black dot at the origin. Each cylinder is represented with its cross-section (circles) with the image plane. Apparently random cylinder positions (A) are treated as a random occupation of the predefined cells of a lattice (B).

Here, the subscript α counts the cells, $1-p$ and p are respectively the probabilities for a given cell to be vacant or contain a vessel. The relaxation effect of this vessel on the spin packet at the origin is denoted here as ψ_α.

Equation (16) can be given a form, which is similar to the basic formula Eq. (13) of the model of independent cylinders. To do so, one has to take logarithm of both sides of Eq. (16) and approximate the sum over α by an integral over $\mathbf{x}$. This gives

$$\ln\frac{s}{s_0} = -b_0 D + \int \frac{d^2\mathbf{x}}{\sigma} \ln[1 - p\cdot(1-\psi)], \tag{17}$$

where ψ is now understood as a function of $\mathbf{x}$. This formula is exact in the limit of vanishing cell size, which is not implied in general.

The generalization of the model for the randomly oriented cylinders is straightforward. One has to add two angular dimensions that define the cylinder orientation and repeat the above calculation for every plane which is rotated according to a selected grid in angle space. In-plane occupation probability p should be reduced according to the increased number of available orientations. The value of p can be considered as a constant for all cells in the four-dimensional lattice (consisting of two angular and two in-plane dimensions). The sufficient conditions for that would be the isotropic vessel distribution, the cells with equal area and equal solid angle in the angular lattice. This results in the same signal form as in Eq. (16), but with α counting all cells in the four-dimensional lattice. Finally, the summation over vessel orientation is replaced with an integration resulting in the same angular integral as in Eq. (13) to appear in Eq. (17) (see Eq. (18) below). This construction eliminates the configurations with coinciding vessels, but still allows for crossing of non-parallel vessels. As shown below, this is sufficient for the consistency of the model.

The model parameters p and σ are related to the volume fraction of vessels. Indeed, $\zeta = pz$, where $z = \pi\rho^2/\sigma$ is the filling factor, which is the fraction of volume occupied by the vessel centered in its cell. Substitution of $p = \zeta/z$ in Eq. (17) yields the basic equation of the model of mutually avoiding cylinders:

$$\ln\frac{s}{s_0} = -b_0 D + z\int \frac{do}{4\pi}\int \frac{d^2\mathbf{x}}{\pi\rho^2} \ln\left[1 - \frac{\zeta}{z}(1-\psi)\right]. \tag{18}$$

Logarithm in this formula can be expanded when $\zeta\cdot(\psi-1)/z \ll 1$ giving the previously known result Eq. (13) for the model of independent cylinders. With the strong diffusion weighting, ψ becomes exponentially large in certain regions of $\mathbf{x}$. In this case, Eq. (18) should be used, in which the increase in ψ is reduced by the logarithm, while the theory based on the model of independent cylinders Eq. (13) fails.

Parameter z enters the result although the explicit lattice is not represented in the integration in Eq. (18). For

the continuous vessel distribution, z shows how close two neighboring vessels are allowed to be. The lower bound on z is set by the restriction $z > \zeta$, since $p < 1$. Near this limit the vessels form an almost regular patten with $p \approx 1$, which reminds of the lattice put in the model origin. The larger is z, the more independent the vessel positions are. The distribution of distances between the closest neighbours becomes broader. For $z > 1$ a partial vessel overlap is allowed. In the limit $z \to \infty$, the vessels become statistically independent and Eq. (18) turns into Eq. (13).

7. Results for model of mutually avoiding cylinders

Integration in Eq. (18) was performed numerically in the way similar to calculation of the vessel dephasing effect described in [7]. A comparison with the model of independent cylinders is presented in Fig. 5. The divergence seen in Fig. 3 disappears in agreement with the above discussion. The residual z dependence indicates that the signal is sensitive to the mutual correlations in the vessel positions. There is currently no theoretical estimate available for the value of z. This parameter should be rather low to restrict the overlapping of cylinders. For the following estimates the values $z = 1.4\zeta$ and $z = 2\zeta$ are used. The former is found from comparison with experimental data as described below.

Typical results for realistic tissue parameters are shown in Fig. 6. All lines in the figure are nearly straight lying above the product $-b_0D$. The measurement results, if treated in the common way, would lead to an underestimation of the diffusion coefficient. The relative error is a slightly increasing function of b_0D for all data shown in Fig. 6. The correction should decrease again for very strong weighting for which the applied gradient

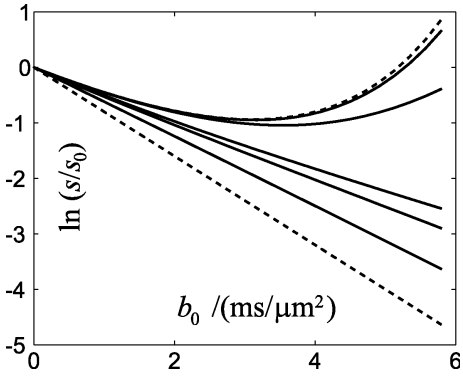

Fig. 5. The same as in Fig. 3 for the model of mutually avoiding cylinders. The upper dashed line reproduces the prediction for the measurement with the contrast agent enhancement shown in Fig. 3. The lower dashed line shows the term $-b_0D$. The solid lines represent results for the same parameters with z taking the following values (from top to bottom): $z = 10$, $z = 1$, $z = 0.1$, $z = 0.07$ (which is $z = 2\zeta$), and $z = 0.038$.

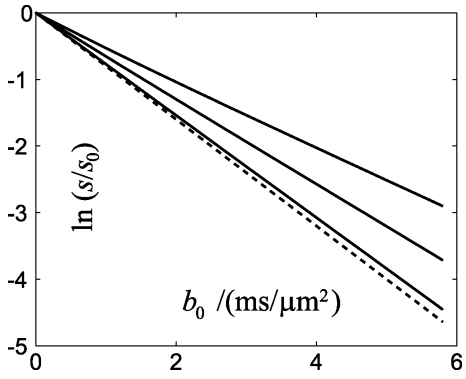

Fig. 6. The same as in Fig. 3 for the model of mutually avoiding cylinders. Three solid lines represent results (from bottom to top) for the following cases: (i) diffusion measurement with the default parameters, the maximal correction to $-b_0D$ is 4%; (ii) for a tissue with the high blood volume fraction $\zeta = 10\%$. The maximal correction to $-b_0D$ is 20%; and (iii) for the measurement with the paramagnetic contrast agent. The maximal correction to $-b_0D$ is 37%.

is much higher than the mesoscopic ones. This is supported by data shown in Fig. 7.

The decrease in the apparent diffusion coefficient seen in Fig. 6 agrees with experimental results [2]. The dependence between the apparent diffusion coefficient in the rat brain ($-\ln(s/s_0)/b_0$ in the present notations) and the intravascular magnetic susceptibility was found to be linear with a coefficient 33%/ppm. The default values defined in Section 2 result in 52%/ppm. The experimental value can be reproduced by adjusting z and by using of the experimental parameters [2] ($B_0 = 2\,\mathrm{T}$, $T_E = 42\,\mathrm{ms}$, $\Delta = 23\,\mathrm{ms}$, $\delta = 8\,\mathrm{ms}$, and $b = 1.35\,\mathrm{ms}/\mu\mathrm{m}^2$). This results in $z = 1.4\zeta$.

The calculation of the mean vessel radius via the averaging of $\rho^{-2/3}$, which was performed in Section 2, employed the theory developed for $G_0 = 0$. Numerical calculations show that the same form of vessel calibre dependence holds for the relative underestimation of

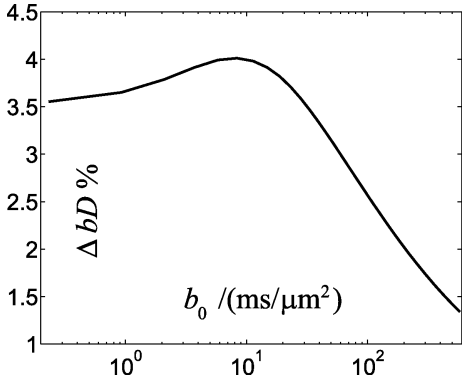

Fig. 7. The per cent correction $\Delta bD = -[\ln(s/s_0) + b_0D]/b_0D$ as a function of b_0 for unrealistically strong diffusion weighting up to $b = 500\,\mathrm{ms}/\mu\ \mathrm{m}^2$ which is examined in order to demonstrate the decrease in ΔbD for strong weighting. Other parameters correspond to the lower solid line in Fig. 6.

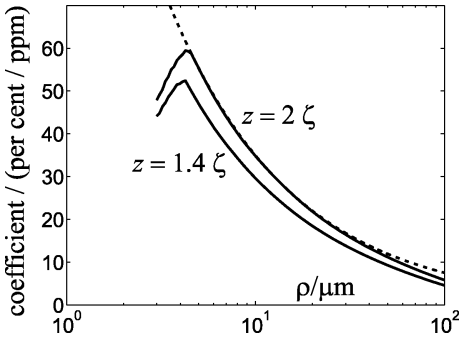

Fig. 8. The coefficient in the liner relationship between the increase in blood magnetic susceptibility and the apparent underestimation the diffusion coefficient shown as a function of radius of monosized vessel population (solid lines). The tissue parameters are set by default values described in Section 2 for contrast enhanced measurements. The measurement parameters corresponds to experiments of [2]. The correlation parameter z takes the values $z = 1.4\zeta$ and $z = 2\zeta$ as indicated. The dashed line shows the dependence $\rho^{-2/3}$, which describes the data well.

the diffusion constant (Fig. 8). This supports the choice of parameters, but this also indicates that the discussed relation between the apparent diffusion and doping blood with paramagnetic contrast is not more sensitive to the vessel calibre than the transverse relaxation of the spin echo.

The model described by Eqs. (10) and (18) possesses scaling rules due the fact that a number of its parameters is combined in two terms in Eq. (10). First note that an increase in the diffusion coefficient by a factor, k, such that $D \to kD$, can be compensated by a simultaneous reduction of all time parameters, δ, Δ, and T_E by a factor $k^{1/3}$. For the unchanging sequence timing, the rescaling $G_0 \to k^{-1/2}G_0$ and $\mathbf{x} \to k^{1/6}\mathbf{x}$ in Eq. (18) with account for Eq. (6) leaves ψ and the b-factor unchanged. This results in an increase in the difference $\ln(s/s_0) + b_0 D$ in Figs. 5 and 6 by a factor $k^{1/3}$. The dependence on the echo and diffusion time can be evaluated in a similar way.

8. Discussion

The developed model of mutually avoiding cylinders is embedded in the framework of existing theory of transverse relaxation in biological tissues [5–7]. The model interpolates between the independent placing of cylinders, which simulate the vessels, and their correlated positions. In the limiting case of strong correlation the vessel form a lattice, which is hidden in the integral in Eq. (18). The integration should correctly reflect the dependence on involved parameters, but result in differences in numerical coefficients as compared with the summation over specific lattices. The lattice results can be found directly from Eq. (16), but it would be of little practical help unless the genuine microvascular architecture displays the corresponding regularity. It is known that the capillary positions are indeed correlated [12] making the distance between them less varying as it would be for their independent placement. This can be understood as a mechanism for the maximal homogeneity in the oxygen supply. This property gives credit to the above found value $z = 1.4\zeta$, which indicates significant correlations in the mutual vessel positions.

Present results demonstrate that the signal attenuation in diffusion measurements is sensitive to the architecture of microvascular network. This goes in line with the sensitivity of transverse relaxation to the structure of paramagnetic objects that induce the mesoscopic gradients [13,14]. In the present context the effect is due to the unsuppressed signal from a number of mesoscopic regions in which the field of specifically arranged nearest vessels compensates for the applied gradient. In the model of independent cylinders, these regions dominate the signal in spite of their low statistical weight. In the model of mutually avoiding cylinders, which results in the logarithm in Eq. (18), there is no dominant contribution, but the dependence on the correlation in vessel positions holds.

The results obtained show the capability of diffusion to probe the microvascular architecture when combined with the enhancement of mesoscopic gradients by an intravascular contrast agent. Exploring the mesoscopic structure is currently considered as a prerogative of diffusion [15–17]. The underlying mechanism is the restriction of diffusion imposed by the investigated structure. It takes effect at distances of the order of the diffusion length. Another kind of examination is enabled by the paramagnetism of the mesoscopic sub-structure. The induces magnetic fields cause an increase in the transverse relaxation, which is sensitive to the shape of the field source [13], though this sensitivity is mediated by an effectively short-ranged interaction [14]. In contrast, the proposed mechanism makes use of diffusion as a local probe of long-ranged magnetic fields the extent of which is larger than the diffusion length.

9. Conclusion

It is demonstrated theoretically that the susceptibility contrast between the intra and extravascular compartments in perfused biological tissues results in an underestimation of apparent diffusion coefficient. The effect is shown to be small for realistic tissue and NMR parameters, but it is appreciable in blood enriched organs such as liver or under enhancing the blood paramagnetism with a contrast agent. The correction magnitude turns to be sensitive to the mutual correlations in the vessel positions, which are characterised by a new parameter, the value of which is found in comparison with experi-

mental data. Developed theory agrees with experimental results [2] obtained in the rat brain.

Acknowledgments

I am grateful to K. Il'yasov, D.S. Novikov, D.A. Yablonskiy, and M. Zaitsev for help and useful discussions. An initial part of this work has been done at Institute of Medicine, Research Center Jülich, Germany.

References

[1] J. Zhong, R.P. Kennan, J.C. Gore, Effects of susceptibility variations on NMR measurements of diffusion, J. Magn. Reson. 95 (1991) 267–280.
[2] M.D. Does, J. Zhong, J.G. Gore, In vivo measurement of ADC change due to intravascular susceptibility variation, Magn. Reson. Med. 41 (1999) 236–240.
[3] R.F. Karlicek, I.J. Lowe, A modified pulsed gradient technique for measuring diffusion in the presence of large background gradients, J. Magn. Reson. 37 (1980) 75.
[4] K.A. Il'yasov, J. Hennig, Single shot RARE sequence with multiple diffusion weighted preparation period: reduction of the artifacts and the sensitivity to background gradients, Proc. Int. Soc. Magn. Reson. Med. Sidney (1998) 657.
[5] D.A. Yablonskiy, E.M. Haacke, Theory of NMR signal behavior in magnetically inhomogeneous tissue: the static dephasing regime, Magn. Reson. Med. 32 (1994) 749–763.
[6] V.G. Kiselev, S. Posse, Analytical theory of susceptibility induced NMR signal dephasing in a cerebrovascular network, Phys. Rev. Lett. 81 (1998) 5696–5699.
[7] V.G. Kiselev, S. Posse, Analytical model of susceptibility-induced MR signal dephasing: effect of diffusion in a microvascular network, Magn. Reson. Med. 41 (1999) 499–509.
[8] Le Bihan D, Turner R, Patronas N. Diffusion MR imaging in normal brain and in brain tumor. In book [16].
[9] W.M. Spees, D.A. Yablonskiy, M.C. Oswood, J.H. Ackerman, Water proton MR properties of human blood at 1.5 Tesla: magnetic susceptibility, T_1, T_2, T_2^*, and non-Lorenzian signal behavior, Magn. Reson. Med. 45 (2001) 533–542.
[10] V.G. Kiselev, On the theoretical basis of perfusion measurements by dynamic susceptibility contrast MRI, Magn. Reson. Med. 46 (2001) 1113–1122.
[11] E.O. Stejskal, J.E. Tanner, Spin diffusion measurements: spin echos in the presence of a time-dependent field gradient, J. Chem. Phys. 42 (1965) 288–292.
[12] G. Pawlik, A. Rackl, R.J. Bing, Quantitative capillary topography and blood flow in the cerebral cortex of cats: an in vivo microscopic study, Brain Res. 208 (1981) 35–58.
[13] V.G. Kiselev, D.S. Novikov, Transverse NMR relaxation as a probe of mesoscopic structure, Phys. Rev. Lett. 89 (2002) 278101.
[14] V.G. Kiselev, D.S. Novikov, Kiselev and Novikov reply, Phys. Rev. Lett. 91 (2003) 029802 (A Reply to the Comment by Y.-Q. Song and P.N. Sen. Ibid, 029801).
[15] P.P. Mitra, P.N. Sen, L.M. Schwartz, P. Le Doussaland, Diffusion propagator as a probe of the structure of porous media, Phys. Rev. Lett. 68 (1992) 3555–3558.
[16] D. Le Bihan, R. Turner, N. Patronas, Diffusion MR imaging in normal brain and in brain tumor, in: D. Le Bihan (Ed.), Diffusion and Perfusion Magnetic Resonance Imaging: Applications to Functional MRI, Raven Press, New York, 1995, pp. 134–140.
[17] D.A. Yablonskiy, A.L. Sukstanskii, J.C. Leawoods, D.S. Gierada, G.L. Bretthorst, S.S. Lefrak, J.D. Cooper, M.S. Conradi, Proc. Natl. Acad. Sci. USA 99 (2002) 3111–3116.